SOME EXPERIMENTAL OBSERVATIONS ON CIRCULATING CURRENTS IN A CROSSED FIELD PLASMA ACCELERATOR

J. Jedlicka* and J. Haacker*

Ames Research Center, NASA

Moffett Field, California 94035

/December 1971/

Backup document for Synoptic scheduled for publication in AIAA Journal, May 1972, under the same title.

*Research Scientist, High Enthalpy Research Branch

ABSTRACT

Experiments on a thermally ionized argon plasma suggest that applying a Lorentz force by means of orthogonal electric and magnetic fields to an electrically conducting fluid flow imposes necessary but not sufficient conditions for acceleration. There are, in fact, many combinations of current and magnetic field which cause decelerations of the fluid. The deceleration arises from a retarding force which may be larger than the applied Lorentz force. The retarding force causing the deceleration is a consequence of currents circulating completely within the fluid. These currents arise from differences in velocity between the central and wall regions of the duct which interact with the imposed magnetic field to produce differences in induced voltages. The observed physical effects of the circulating currents cause a loss in velocity in the central region of the duct, an increase in thermal energy in the sidewall region, and little change in thermal energy near the electrode wall region. For similar velocity profiles, the adverse effects appear to be related to the product of electrical conductivity and velocity, and performance as an accelerator appears to be controlled by the Hoffman loading parameter (i.e., the ratio of the applied to the induced currents).

INTRODUCTION

The J X B accelerator has been explored at Ames Research Center to study the possibility of producing a fluid stream of high velocity and density to be used as a laboratory source of plasma. The final accelerator configuration is shown schematically in Fig. 1. The experimental apparatus consists of a

constricted arc (described in Ref. 1) having a constrictor of 13-mm diameter and 1/2-m in length, which has been coupled through an aerodynamically smooth transition to a crossed-field accelerator, as shown on Fig. 1. The advantage of the constricted arc as a plasma source for the accelerator is that sufficient electrical energy can be added to the plasma before it enters the accelerator so that it may be excited thermally at any enthalpy up to the first ionization level of the chosen gas. When the plasma is expanded through the coupling section between the constricted arc and the accelerator, the gas enters the accelerator with both high velocity and electrical conductivity. For example, values up to 6.3 km/s and 1100 mhos/m can be produced with argon. The main disadvantage of the constricted arc is that the velocity and the electrical conductivity cannot be independently adjusted for a particular species of gas, because both result from the same thermal excitation.

Two scale drawings of the accelerator are shown in Fig. 2. Surfaces in contact with the plasma were segmented copper, shown cross hatched; segmented, anodized aluminum; and a test box bulkhead insulator of boron nitride which was used for its high temperature electrical insulating properties because strength requirements precluded the segmentation of the bulkhead. Prior to the design of the accelerator experiments were made to assess the electrical insulating properties of the surfaces exposed to the plasma and to guarantee that the segment insulation could be indefinitely maintained. Of the several gases tested, surface discharge occurred at the least voltage with an argon plasma; the numbers following are exclusively for argon plasma.

Cold copper segments undergo an abrupt surface discharge when the adjacent segment voltage difference reaches approximately 60 volts, a value which appears to be independent of segment gap for gaps in the order of 1 millimeter. In the stream direction the segmentation varied from 6.3 millimeters in the segmented constrictor, 10 millimeters in the electrode and isolating regions, to 20 millimeters for some of the supersonic transition region. In general the segmentation interval was chosen from experience with an earlier plasma generator and accelerator such that a factor of safety of 3 for surface breakdown would exist on adjacent surface. In the case of water cooled copper surfaces, segmentation was provided for expected plasma potential differences of 20 volts.

If aluminum is anodized until all apparent electrolytic action stops the resulting surfaces maintain their insulating properties until a potential difference of approximately 600 volts is reached. Water cooled anodized aluminum was used for the sidewalls. The design factor of safety on electrical breakdown was deliberately made larger than in the case of copper surfaces to take into account the possibility of undetected surface damage to some local region of the anodized coating.

The accelerator has cross-section dimensions of 5-cm x 5-cm at its upstream end. The top and bottom walls, which diverge to compensate for boundary layer growth, are formed by the electrode and isolating surfaces through which external current is supplied. The magnetic field intensity is adjustable from 0 to 1 Tesla; a typical magnetic field profile is shown in Fig. 2. The nine active electrode pairs consist of water-cooled copper bars, located at 1-cm intervals

in the stream direction and separated from each other by 0.23 mm gaps. These gaps were found by experiment to provide effective cold-gas insulation between electrodes. The water-cooling circuits are arranged on both the constricted arc and the accelerator so that heat-transfer measurements may be made on the various segments of the apparatus. After leaving the accelerator, the stream enters a large test box in which static pressure was maintained equal to accelerator static pressure, and where instruments, 10 millimeters downstrean of the stream exit plane, measure stream centerline velocity, heat transfer, and electrical conductivity. The stream instrumentation is comprised of an optical system which measures the centerline velocity by means of the time of flight of random light variations assumed to be fixed relative to the gas,[2] and three instruments which can be programmed to make profile measurements along the applied magnetic field, B_z, and along the applied electric field, E_y. These include a pitot probe, a local stagnation heat-transfer probe, and a velocity-conductivity probe; the first two yield a calculated stream velocity, following Ref. 3,4, and the latter an independent determination of velocity from σ and σU measurements in the stream.[5] Typical profiles of impact pressure measurements and local stagnation heat-transfer measurements are shown in Fig. 3, for the case of $B_x = J_y = 0$ and for $B_z > 0$, also with $J_y = 0$. These surveys were made in both the X-Z plane and the X-Y plane. A typical profile made with the σU probe in the X-Z plane, for $B_z = 0$, is shown in Fig. 3(e). These curves are reproduced from recording oscillograph traces. In addition wall static pressures were recorded to assist in determining the operating characteristics of the device. Electrical parameters are recorded on a rapid-sequence

camera which photographs panel-mounted meters. Other data are collected on a strip chart recorder. A wide variety of test conditions have been explored; table 1 gives typical stream parameters. In general, the applied current and the applied magnetic field are not interchangeable with respect to the acceleration produced as might be anticipated for a Lorentz force. Velocity increases of 2-1/2 times have been measured; yet there are many combinations of current and magnetic field for which deceleration rather than acceleration occurs. Regimes of poor performance have been predicted in the literature, but generally for the case of the Hall parameter greater than 2 and most infrequently for the open circuit generator case (the Hall parameter was less than 2 in the tests reported herein). Much of the experimental work presented herein was concerned with this problem.

The Effect of a Magnetic Field on a Plasma Stream

Figure 4 shows a typical plot of centerline velocity, U, as a function of the applied magnetic field, B_Z for several values of external current density, J_y. This current density has been calculated by taking the quotient of the applied external current for an electrode and the projected electrode area in the X-Z plane. For many cases, the centerline velocity shows an increase for modest values of B field, but net losses in velocity for larger values. The increase in velocity is only a fraction of that which one would predict from one dimensional theory, also shown in Fig. 4 for comparison. The shape of the experimental curve (first rising and then falling) suggests that there are at least two primary mechanisms within the plasma stream. The Lorentz force tends to produce acceleration, but simultaneously a retarding force exists, nonlinear with respect to B_Z, which

competes with and finally overwhelms the Lorentz force at higher values of B_Z. Open circuit tests were then made to study the competing or retarding mechanism. Most of the tests were made with argon, but a few were made using helium and nitrogen. The helium plasma had the highest velocity and showed the greatest effects when the magnetic field was applied.

A helium plasma, observed at the channel exit in the X-Y plane, before application of an external-magnetic field, displays a well collimated stream, and time-of-flight measurements show its centerline velocity to be 21.4 km/s. At the same operating conditions, a magnetic field strength of 0.4 Tesla was applied, which caused the luminous stream visually to deteriorate into a wide, fan-shaped, plume which generally deflected in the positive y direction, probably due to the Hall effect, with centerline velocity reduced to 5 km/s. The luminous stream visually showed fairly good collimation when viewed in the X-Z plane at the channel exit, for both the $B_Z = 0$ and the $B_Z = .4$ Tesla conditions. It is apparent that the disturbing forces are not scalar in nature as expected from pressure effects, but have definite direction. Argon and nitrogen plasma streams shown the same effects to a lesser degree (see Fig. 3(d)).

The centerline velocity is plotted in Fig. 5, as a function of the applied magnetic field for an argon plasma at three values of electrical conductivity. The electrical conductivity values of 1100, 780, and 290 mho/m, were measured in the absence of an applied magnetic field. The curve for an electrical conductivity of 1100 mho/m, corresponding to the highest velocity, shows the largest velocity decrement with increasement in magnetic field. The curve for 290 mho/m shows a minimal effect. A comparison of the curves on Fig. 5

indicates that velocity strongly affects the retardation forces acting on the stream and suggests that the electrical conductivity also has a strong influence on fluid deceleration at open circuit conditions. Probably some combination of velocity and electrical conductivity cause the deceleration effects. The curves appear to be approaching an asymptote as B_z is increased. This suggests a compensating mechanism such that for large values of magnetic field the retardation force diminishes.

Two experimental points obtained with helium are shown in Fig. 5. The quantity of helium data was limited by severe operational difficulties and apparatus failure involved in using this gas. The two points correspond to velocities of 21.4 km/s at $B_z = 0$ and 5.0 km/s at $B_z = 0.4$ Tesla. Since the stream was not seeded the electrical conductivity and velocity could not be independently controlled, hence helium was run at a much higher velocity than argon at a conductivity of 1100 mho/m. With a magnetic field applied, the velocity of the helium stream decreased such that the velocities of both the helium and argon streams were the same at a magnetic field strength of $B_z = 0.4$ Tesla, further indicating that the absolute value of velocity may be an important parameter affecting the magnitude of the retarding force.

Open circuit voltage measurements were made for a variety of initial plasma conditions. Were the plasma to have a uniform electrical conductivity equal to its centerline value, it would have an internal resistance of the order of 100 milliohms. The cooling water passages attached to the electrodes represent a resistive load of 55 kiloohms and the voltmeter used to measure open-circuit voltage had a series resistance of 300 kiloohms. Assuming a reduced electrical conductivity next to the cold electrode surfaces, the above values suggest that the voltage measurements may be considered as open-circuit values.

Typical open-circuit voltage data are plotted in Fig. 6. The general shape of the experimental curves was verified in preliminary tests in which voltage data were taken for small incremental changes in magnetic field. The straight lines passing through the origin are theoretical U X B curves with a numeric factor of two-thirds applied to account for the parabolic-like velocity profiles which have been measured in the E_y direction. The open-circuit voltage appears to have a correspondence with the velocity data shown in Fig. 5. For very low values of applied magnetic field, the open-circuit voltage may approach the theoretical value. It was found that this limit was 5 milli Teslas for somewhat different test conditions.[6] As the applied magnetic field is increased, a pronounced departure from the theoretical open-circuit voltage appears. There is even a region in which the open-circuit voltage appears to diminish as the magnetic field is increased. Such a voltage minimum appears in the data of Ref. 6 and has been reported in Ref. 7 for a seeded helium stream. Finally at the highest values of the magnetic field some corrective or favorable action appears to have taken place such that the open-circuit voltage again appears to be rising, but always at a slope small compared to that which would be predicted by one-dimensional theory. Open circuit voltage of only a fraction of the generated voltage $UB_z h$ and having a variation with magnetic field showing a dip followed by a rise at lower slope has been reported for a seeded MHD generator in Ref. 8.

Heat transfer was measured for the open circuit generator case for $\underline{B}$ field values from 0 to 0.5 Tesla; the data are plotted on Fig. 7. The reason for the differences in heat transfer rate in the absence of $\underline{B}$ field is not known. The

maximum in anode wall heat transfer rate, $\underline{B}$ = 0.2 Tesla, corresponds to the maximum deflection of the luminous plasma stream, in the direction toward the anode wall, observed visually. It is apparent that the electrically insulated sidewalls are much more affected by the magnetic field. Note also that the effect of the magnetic field diminishes at the highest field strengths.

In the classical Hartmann analysis, circulating currents were assumed to enter and leave electrode walls. In contrast to this, a model was assumed in Ref. 9 in which the circulating currents closed completely within the stream rather than include the electrode walls as part of the current path. It should be possible to distinguish between the two models by means of experimental measurement because the Hartmann model should include sheath drops at the plasma-electrode interface, whereas the model of Ref. 9 should not. The sheath drops would produce additional heat transfer to the electrode walls. The magnitude of the additional heat transfer can be predicted from the accelerator experiments in which external current is applied, and the additional heat transfer is about the same magnitude as the convective heat transfer (that is, when external current is applied for operation as an accelerator, the incremental increase in heat transfer to the electrode walls is approximately twice that to the sidewalls).

The electrode wall data of Fig. 7 show little change with increase in magnetic field strength, in agreement with the theory of Ref. 9 for circulating currents closing completely within the fluid. This result could have been predicted from Steenbeck's Minimum Voltage Principle,[10] which states that an electrical discharge will choose that path which will make its voltage a minimum. The

sheath voltages are equivalent to a large path length of plasma, for equal voltage drop, so that current could be expected, in general, to circulate completely within the fluid, rather than to follow the classical Hartmann model.

Figure 8, redrawn from Ref. 9, illustrates schematically the internally circulating currents. This model predicts a retardation of the central portion of the plasma stream, and an acceleration of the stream in the vicinity of the side walls. Obviously, the acceleration in the vicinity of the side walls must increase the viscous losses and result in a net loss of stream momentum. The magnitude of these losses should be of interest.

To investigate this question, stagnation heat-transfer measurements and pitot-probe measurements were made on the stream centerline for the particular set of conditions shown in Fig. 9(a). The stagnation heat-transfer and pitot and static measurements can be combined to provide a velocity as described in Ref. 3 and 4. This velocity is plotted against applied magnetic field. For the same set of stream conditions orthogonal traverses of the pitot probe were made and from these the total stream momemtum or thrust was computed and is plotted in Fig. 9(b).

The model shown in Fig. 8 would, in the absence of viscous losses, predict an increase in stream momentum next to the side walls numerically equal to the decrease in momentum in the central region, with no net overall change in stream momentum. The experimental data, Fig. 9(b), did not confirm this. Figure 9(b) to the contrary, shows that there was a net loss in stream momentum, which paralleled, percentage-wise, the centerline velocity loss. This result is

implicit in the heat transfer analysis of the data shown in Fig. 7 which was made by G. Carlson[9] using his model shown in Fig. 8. He demonstrated that he could predict reasonably well the heat transfer rate changes of Fig. 7 if he assumed that all of the Joule heating produced by the current flow in the vicinity of the insulator walls would appear as heat transferred to the wall. If the circulating currents in fact flow in such close proximity to the insulator side wall as to result in essentially all of the Joule heat appearing as heat transferred to the side walls, then it could reasonably be expected from the Reynolds analogy that the accelerating body force would also be lost through viscous effects at the side walls.

There is additional experimental evidence which supports the idea that the circulating currents flow in close proximity to the side walls. The circulating currents include a Hall component, so that the Lorentz force is not aligned with the x axis but tilted in the positive y direction. This causes the observed flow deflection. In Ref. 9 it is pointed out that this should decrease the heat transfer to the cathode wall and increase it to the anode wall, as found in these experiments (Fig. 7). The Hall effect should deflect the plasma stream downward (the +y direction), in the central portion of the stream and upward (the -y direction), in the side wall regions. In the experiment the stream was deflected downward in the central region, Fig. 3(c), but shows no tendency to deflect upward in the side wall regions. The stream deflection, easily observed visually and by pitot probe measurements, is maximum when the effect on open-circuit voltage and heat transfer is maximum, Figs. 6 and 7, and is much reduced at high values of

magnetic field. This is further evidence that the side wall currents must flow in a thin layer adjacent to the side walls, so that the Lorentz force is absorbed by viscous shear forces at the wall.

The experimental evidence cited thus far will also fit the model commonly referred to as "end looping," that is, decelerating current loops which flow in the plane perpendicular to the magnetic field vector from within the generator magnetic field to outside of the magnetic field (both upstream and downstream). The end loop model has the same driving potential as that of G. Carlson, $\underline{U}x\underline{B}$. The usual apparatus has a length large in comparison to its width and height dimension, so that the path length for end loop currents would be larger than that of the Carlson model. The path resistance would be approximately proportional to the path length, so the end loop current path should have greater resistance than the path for the Carlson model; the end loop current should be therefore correspondingly smaller.

The Effect of External Power on Stream Characteristics

The experimental evidence given in the preceding sections suggests that a crossed-field accelerator should be analyzed similarly to the treatment given the MHD generator by Hoffman, (Ref. 11) and others who recognized the first-order effects of transverse circulating currents. The driving potential for the circulating currents will be measured by the differences in local values of velocity in the z direction; for simplicity these will be assumed proportional to the product of the centerline velocity and the magnetic field density, U X B, and the local current density will be euqal to σ(U X B). This current density

may be comparable to, and will compete with, any externally applied current density, J_y. Hoffman[11] first defined the dimensionless quotient $J/\sigma UB$ as the loading parameter for the MHD generator. Now the vector product of this circulating current density with the applied magnetic field produces a retarding force per unit volume analogous to the Lorentz force per unit volume, J X B. The operation of an accelerator, then, may be viewed as a competition between two forces, J X B which produces an increase in stream momentum, and σ(U X B) X B, which produces a decrease in stream momentum. This relationship is expressed below.

Momentum change = accelerating force - retarding force

$$\Delta U \dot{m}/wh\ell = C_2 \, J \times B - C_1\sigma \, (U \times B) \times B \qquad (1)$$

ΔU is the incremental increase in velocity; $\dot{m}$, the bulk mass flow rate; ℓ, h, w the channel dimensions in the x, y, and z directions, respectively. If the current density, J, is defined as the external applied current per electrode divided by the electrode area projected into the X-Z plane, only a portion of this current could be expected to flow through the central region and contribute to acceleration. An experimental coefficient, C_2, could then be expected to apply to the Lorentz force term. Similarly only a fraction, C_1, of the retarding force would be effective in the central region of the stream. In the case of the open-circuit generator, the first term vanishes, and equation (1) would appear to predict a retarding force which would increase with the square of the magnetic field. Such a square law agrees with experiment for low values of B, Fig. 5,

but does not account for the ameliorative effect at high B which was discussed previously. To match the experiment some mechanism which would cancel the B^2 term at high values of B is needed.

The required mechanism can be found in the electrical conductivity, σ. The controlling value will likely be that in the y direction, orthogonal to the magnetic field. For this case the reduced conductivity is

$$\sigma = \sigma_o (1 + \beta^2)^{-1} = \sigma_o (1 + C_3 B^2)^{-1} \tag{2}$$

where β is the Hall parameter and C_3 is a constant relating the Hall parameter to the magnetic field strength.

If Eq. (2) is introduced into Eq. (1) the retarding force will have the experimentally observed effect. It will be proportional to B^2 for low values of B and approach a constant for larger values.

If Eqs. (1) and (2) are applied to the top curve, Fig. 4, a reasonable fit to the curve will be found for $C_1 = 0.05$; $C_3 = 6.7$.

The Hoffman loading parameter, L, and the interaction parameter, I, can be introduced

$$L = J/\sigma UB; \quad I = \ell \sigma B^2/\rho U$$

These can be included in Eq. (1).

$$(\Delta U/U)(1/I) = -C_1 + C_2 L \tag{3}$$

The velocity, U, which appears in the three dimensionless groupings in Eq. (3) is the exit centerline velocity.

Experimental data can be expressed in the dimensionless groups on the left of Eq. (3) and plotted against the Hoffman loading parameter, L. If the analysis is reasonable, the data should fall on a straight line of intercept $-C_1$ and slope C_2. Experimental data from argon runs of a wide variety of parameters are plotted on Fig. 10. The straight line shown has a slope $C_2 = 0.64$.

More than half of the 25 experimental measurements plotted in Fig. 10 appear at the ordinate intercept and were obtained for the $L = J = 0$ case (the open-circuit generator case). The important effect of augmentation of electrical conductivity by flow of applied current has been neglected; also, viscous effects have been neglected and a curve of wider generality than shown in Fig. 10, may require a viscosity-dependent dimensionless grouping such as the Hartmann or the Reynolds number.

Operation of the accelerator at high values of σ and U, corresponding to the circular data points (B_z and $J_y > 0$), produced little acceleration and in some cases deceleration; this occurred at low values of the loading parameter, corresponding to high values of the σU product. The levels of B_z and J_y at these points are at the maximum capability of the accelerator. Hall shorting between electrodes limited the values of applied magnetic field and electrode erosion limited the current density. For the same value of externally applied power, large accelerations were measured for low values of σU product; this corresponds to a large loading parameter.

CONCLUDING REMARKS

The performance of MHD accelerators, pumps and generators is degraded by circulating currents within the gas stream. These currents exist whenever a magnetic field is applied transverse to an electrically conducting stream with an electrically conducting boundary layer. In the work described herein, the circulating currents have been studied by means of velocity, heat transfer, pitot pressure, and open-circuit voltage measurements and observations of stream deflection. These measurements support Carlson's model of circulating currents which close completely within the fluid and flow in close proximity to the channel side walls. The circulating currents result in output voltages lower than simple theory predicts in the case of the generator, and momentum increases less than that predicted by simple theory in the case of the pump or the accelerator. Although the experiments reported herein were made mainly on a thermally ionized argon plasma, the adverse effects of circulating currents have also been reported for seeded streams. Successful operation of these MHD devices depends on whether a satisfactory solution can be found to eliminate or suppress these effects on the stream.

NOMENCLATURE

J = current density

B = magnetic field strength

E = electric field strength

σ = electrical conductivity

L = Hoffmann loading parameter (defined in text)

I = interaction parameter (defined in text)

U = stream velocity

H = total enthalpy

C_1, C_2, C_3 = constants (defined in text)

ℓ = channel length (x-direction)

h = channel height (y-direction)

w = channel width (Z-direction)

$\dot{m}$ = bulk fluid mass flow

P_s = static pressure

P_{t_2} = impact pressure

Subscripts

x, y, z = coordinate axes shown in Fig. 1

REFERENCES

1. Stine, H., Watson, V., and Shepard, C.: Effect of Axial Flow on the Behavior of the Wall-Constricted Arc, AGARDograph No. 84, pt. 1, Sept. 1964, pp. 451-485.

2. Winkler, E., and Griffin, R.: Measurements in a Frozen, Partially Dissociated High-Speed Gas Stream, Paper presented at the Second Symposium on Hypervelocity Techniques, Denver, Colorado, March 19-20, 1962.

3. Marvin, J.; and Deiwert, G.: Convective Heat Transfer in Planetary Gases. NASA TR R-224, 1965.

4. Marvin, J.; and Akin, C.: Pressure and Convective Heat Transfer Measurements in a Shock Tunnel Using Several Test Gases. NASA TND-3017, 1965.

5. Vendell, E., Posch, R., and Cook, G.: A Coaxial, Three-Coil Probe for Measuring Local Values of Electrical Conductivity and Velocity in Plasma Streams, AIAA Paper 69-327, presented at the 4th Aerodynamic Testing Conference, Cincinnati, Ohio, April 28-29, 1969.

6. Clayden, W.: Langmuir Probe and Velocity Measurements in the ARDE Plasma Jet. Paper given at the AGARD Specialists' Meeting, "High Temperature Aspects of Hypersonic Flow," T.C.E.A., Rhode St. Genese, Belgium, April 3-6, 1962.

7. Schneider, R., and Wilhelm, H.: Experimental Investigation of Closed-Loop MPD Power Generation. Electricity From MHD, Vol. II, Proceedings of a Symposium, Salzburg, Vienna, July 4-8, 1966.

8. Vedenov, A.: Report on a Round Table Discussion on Closed Cycle Systems, Section 2, p. 808, Electricity from MHD, Vol. II, Proceedings of a Symposium, Salzburg, July 4-8, 1966.

9. Carlson, G.: Circulating Currents in Linear Crossed-Field Generators and Accelerators, NASA TN D-5244, May 1969.

10. Peters, T.: Bogenmodelle und Steenbeckiches Minimum-prinzip., Proc. 5th International Conf. on Ionization Phen. in Gases, Munich, Aug.-Sept. 1961, Vol. 1, pp. 885-896. English Translation: Ronson, H.: RAE Library Translation No. 1041, Aug. 1963.

11. Hoffman, M.: Nonequilibrium MHD-Generator Losses Due to Wall and Insulator Boundary-Layer Leakages. AIAA Journal, Vol. 6, No. 9, September 1968.

Table 1.

Typical stream parameters for argon, centerline values, B = J = 0.

σ, mho/m	H, MJ/kg	Mach No.	P_s, N/m^2	P_{t_2}, N/m^2	$\dot{m}$, kg/s	U, km/s
290	7.19	3.28	353	5740	$3.67 \cdot 10^{-3}$	3.35
780	14.6	3.72	300	6230	$3.67 \cdot 10^{-3}$	4.89
1100	18.1	4.49	332	9720	$3.65 \cdot 10^{-3}$	5.60

LIST OF FIGURE TITLES

Figure 1. Schematic of accelerator apparatus.

Figure 2. Scale drawing of accelerator apparatus and typical magnetic field profile.

Figure 3. Typical impact pressure, local stagnation heat-transfer and σ and σU survey profiles across an argon plasma stream at channel exit.

(a) Impact pressure survey X-Z plane; (b) Heat rate survey X-Z plane; (c) Impact pressure survey X-Y plane; (d) Heat rate survey X-Y plane; and (e) σ and σU survey X-Z plane, $B = 0$.

Figure 4. Accelerator performance as a function of magnetic field intensity for several values of applied current density.

Figure 5. Effect of a magnetic field on the velocity of a plasma stream.

Figure 6. Effect on a magnetic field on open-circuit generator voltage.

Figure 7. Effect of a magnetic field on accelerator wall heat transfer rate, open circuit generator conditions.

Figure 8. Origin and flow path of circulating currents.

Figure 9. Comparison of centerline velocity and thrust as a function of magnetic field intensity in an argon plasma.

Figure 10. Accelerator performance expressed as the product of the velocity ratio and the reciprocal of the interaction parameter plotted as a function of the Hoffman loading parameter.

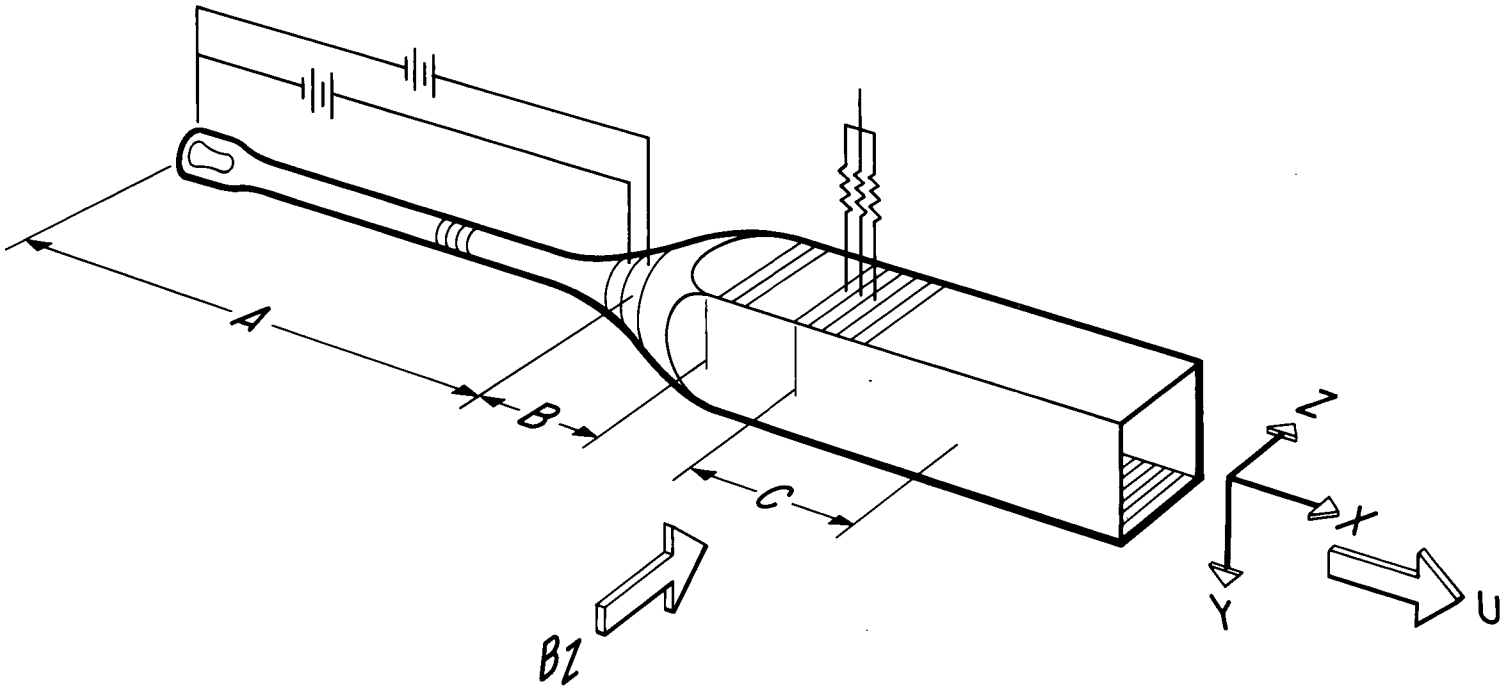

A - CONSTRICTED ARC
B - SUPERSONIC TRANSITION SECTION
C - ACCELERATOR SECTION

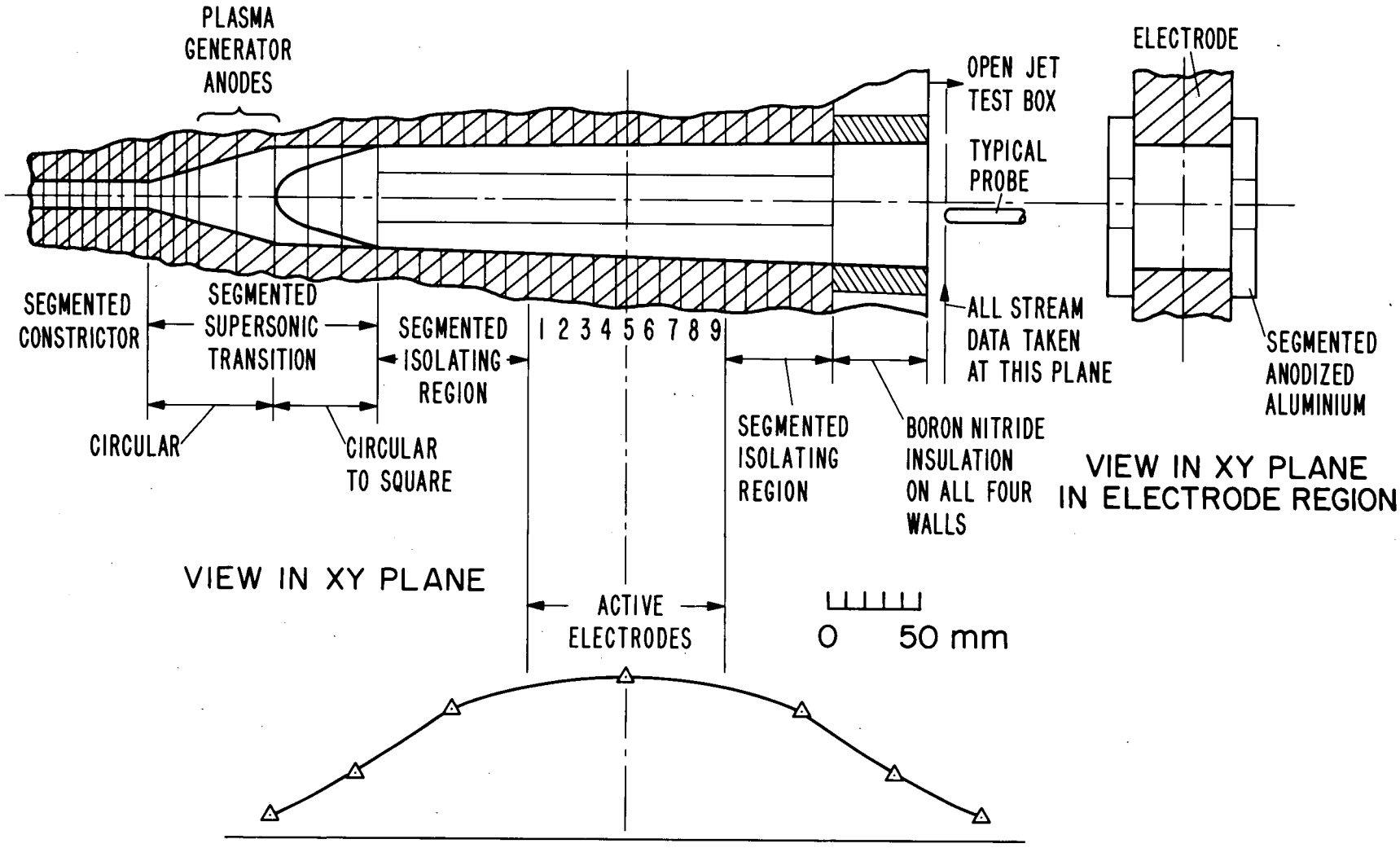

TYPICAL MAGNETIC FIELD PROFILE

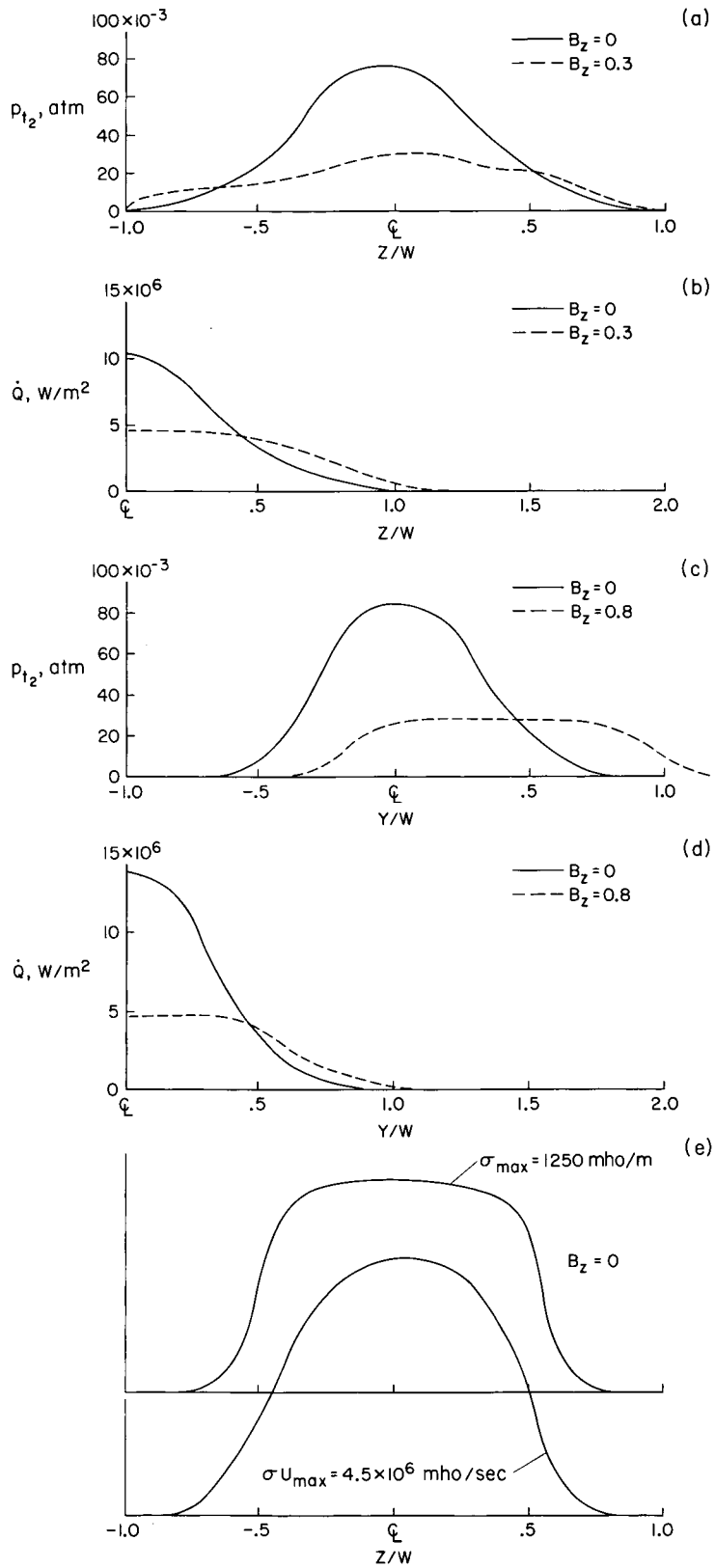
(a)
100×10⁻³
80
60
40
20
0
p_{t_2}, atm
$B_z = 0$
$B_z = 0.3$
-1.0
-.5
℄
.5
1.0
Z/W
(b)
15×10⁶
10
5
0
$\dot{Q}$, w/m²
$B_z = 0$
$B_z = 0.3$
℄
.5
1.0
1.5
2.0
Z/W
(c)
100×10⁻³
80
60
40
20
0
p_{t_2}, atm
$B_z = 0$
$B_z = 0.8$
-1.0
-.5
℄
.5
1.0
Y/W
(d)
15×10⁶
10
5
0
$\dot{Q}$, w/m²
$B_z = 0$
$B_z = 0.8$
℄
.5
1.0
1.5
2.0
Y/W
(e)
σ_{max} = 1250 mho/m
$B_z = 0$
$\sigma U_{max} = 4.5 \times 10^6$ mho/sec
-1.0
-.5
℄
.5
1.0
Z/W

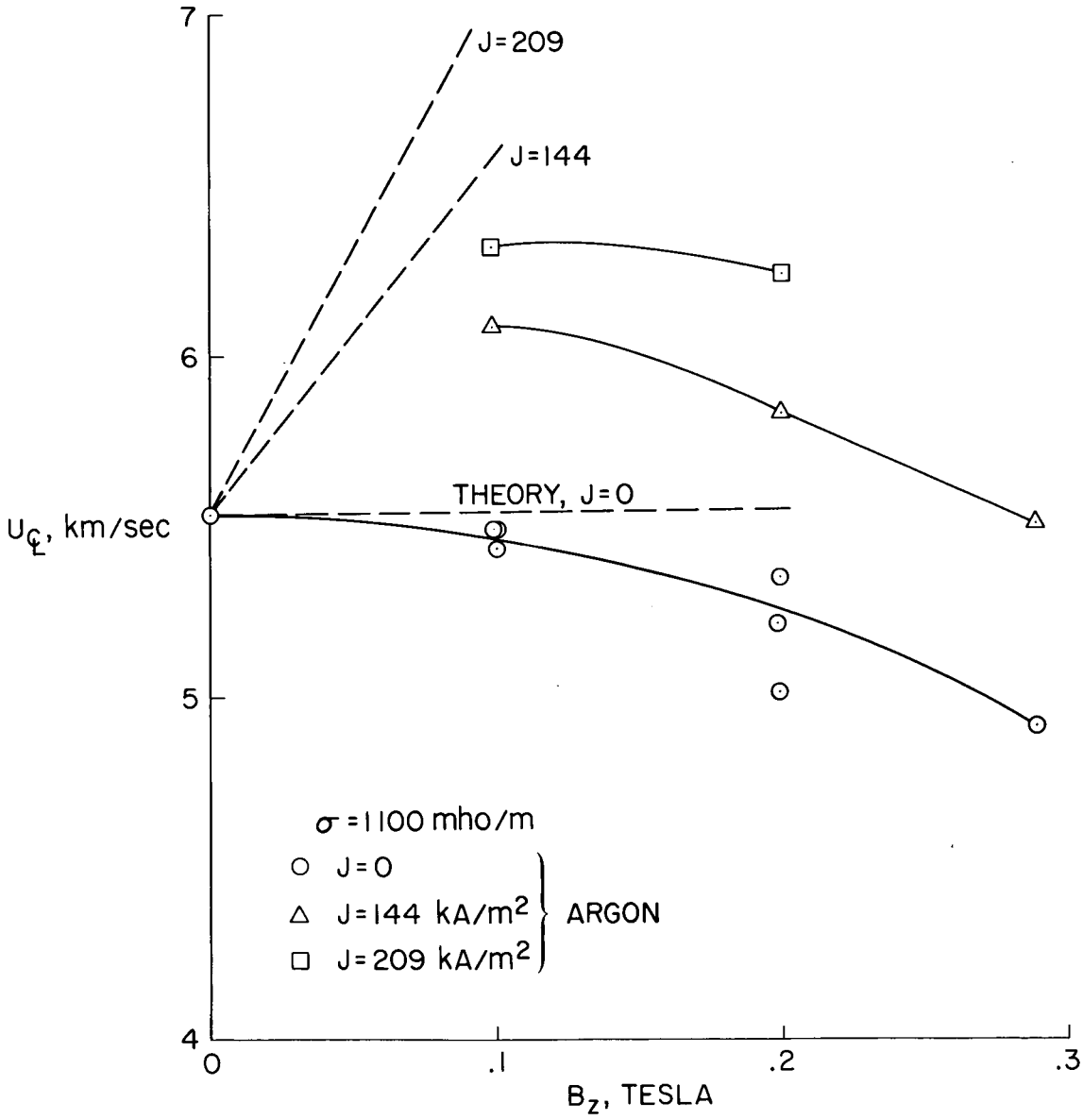
7
6
5
4
J=209
J=144
THEORY, J=0
$U_{\mathcal{L}}$, km/sec
σ = 1100 mho/m
J=0
J=144 kA/m²
J=209 kA/m²
ARGON
0
.1
.2
.3
B_z, TESLA

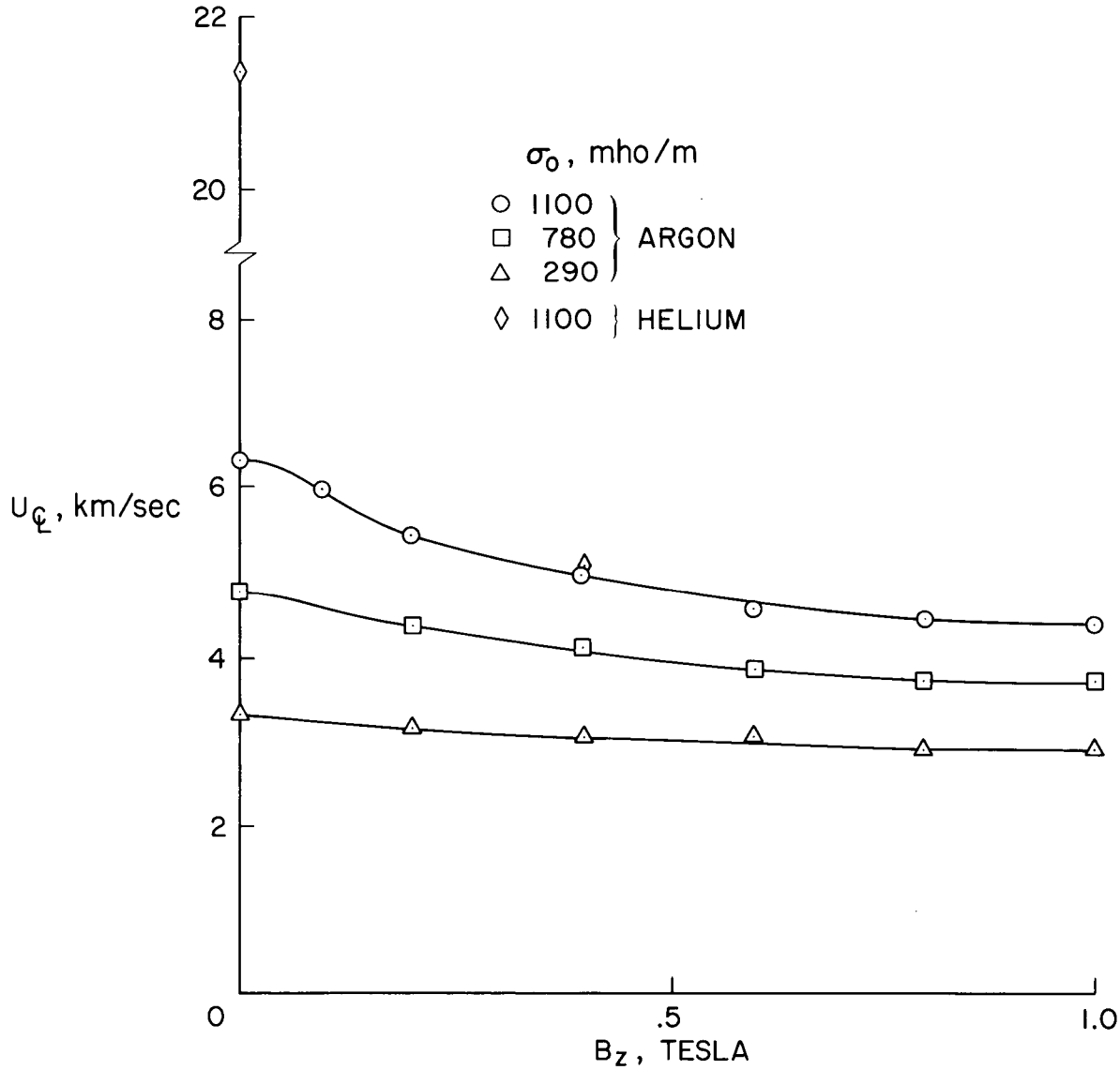
22
20
8
6
4
2
0
.5
1.0
σ_0, mho/m
1100
780
290
ARGON
1100
HELIUM
$U_{\mathcal{L}}$, km/sec
B_z, TESLA

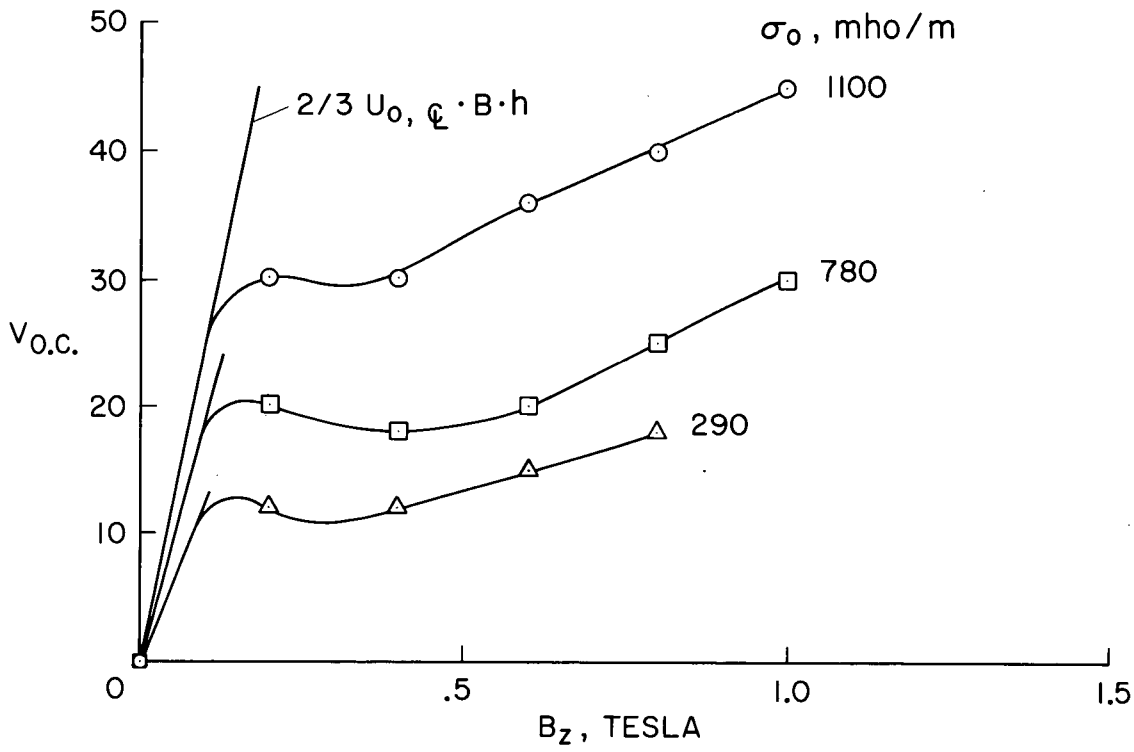
50
40
30
20
10
0
$V_{o.c.}$
σ_o, mho/m
1100
780
290
2/3 U_o, ℄ · B · h
.5
1.0
1.5
B_z, TESLA

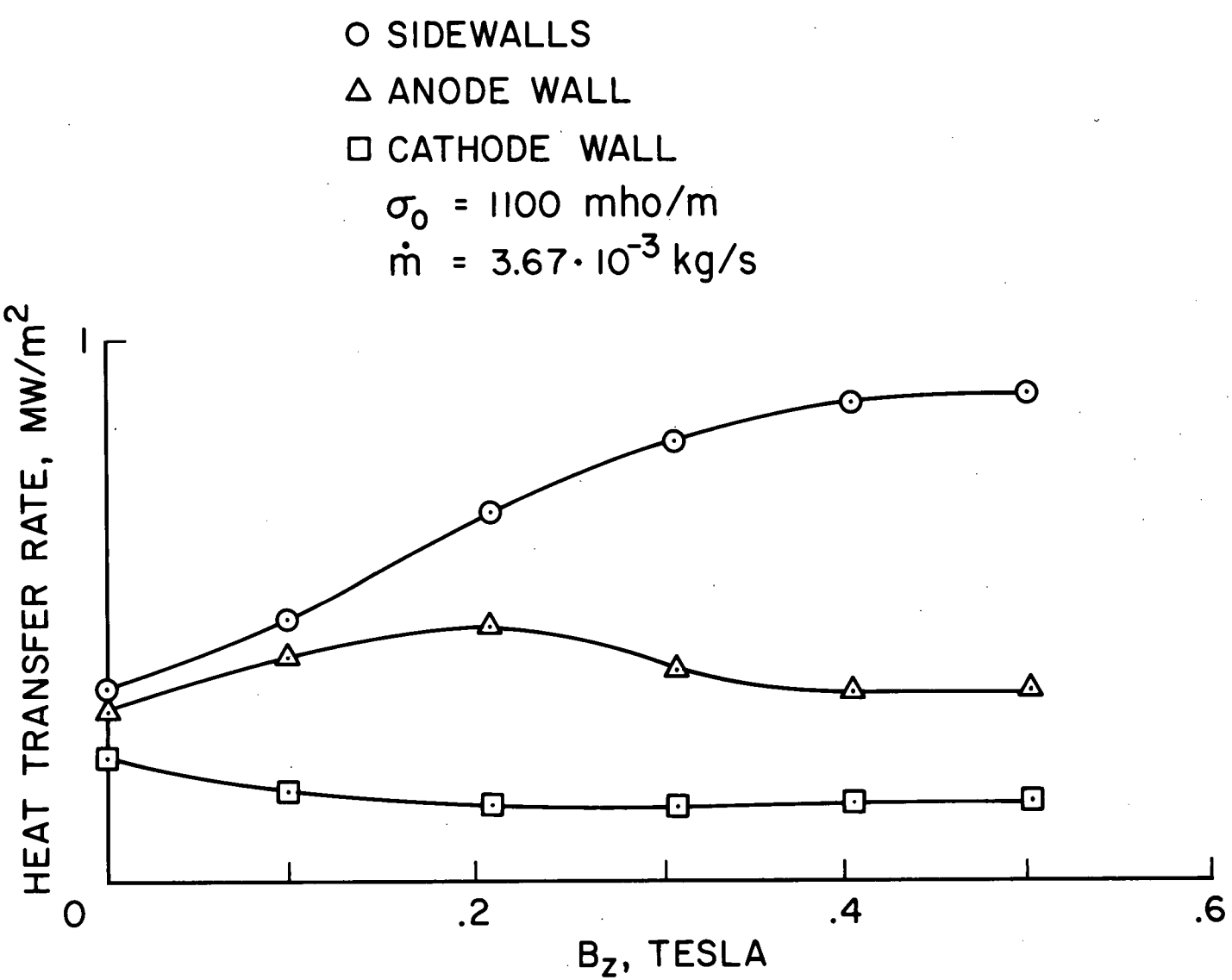
O SIDEWALLS
Δ ANODE WALL
□ CATHODE WALL
σ_0 = 1100 mho/m
$\dot{m}$ = 3.67 · 10^{-3} kg/s
HEAT TRANSFER RATE, MW/m^2
0
.2
.4
.6
B_z, TESLA

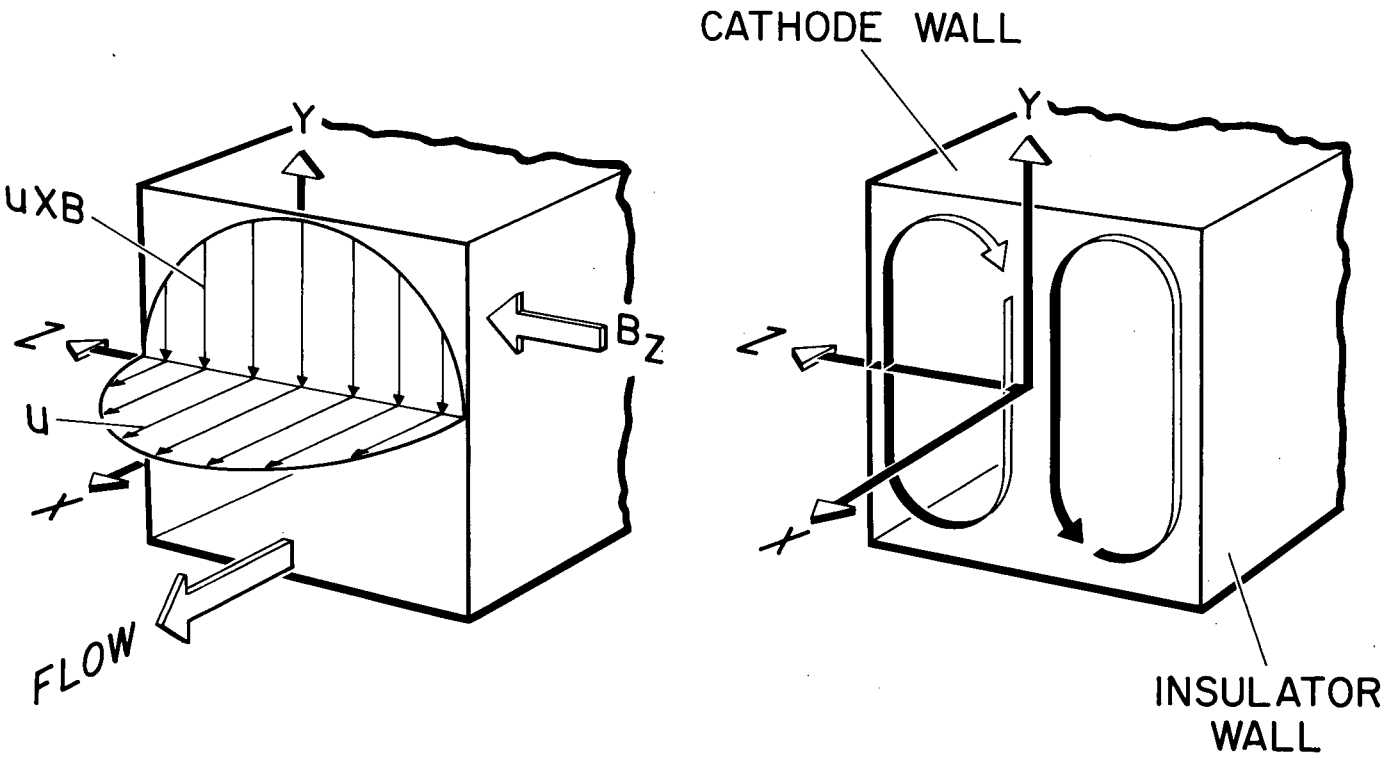
Y
uXB
Z
B_Z
u
X
FLOW
CATHODE WALL
Y
Z
X
INSULATOR
WALL

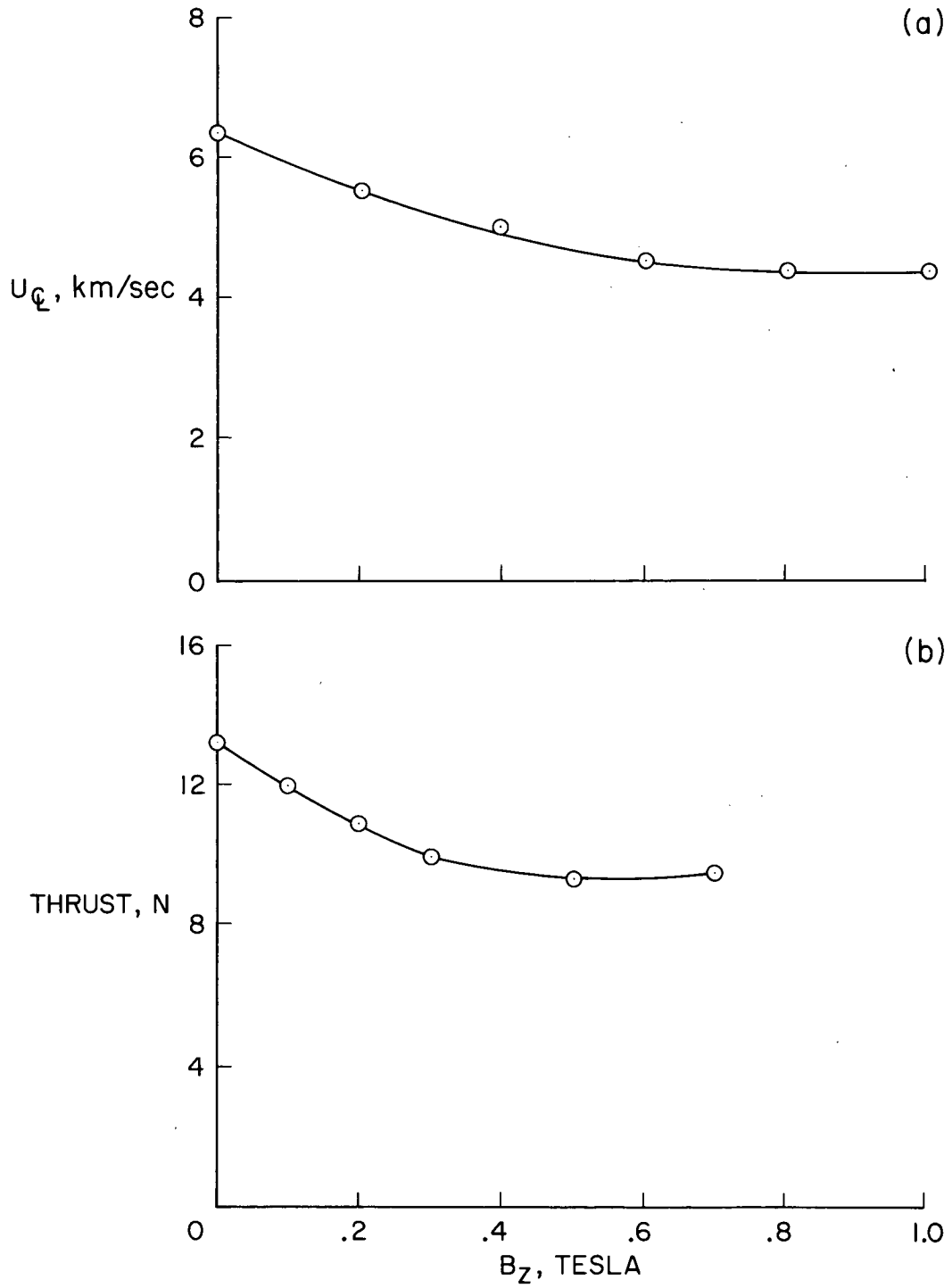
(a)
8
6
4
2
0
$U_{\mathcal{L}}$, km/sec
(b)
16
12
8
4
0
THRUST, N
.2
.4
.6
.8
1.0
B_Z, TESLA

	VELOCITY, km/sec	CONDUCTIVITY, mho/m	FLOW RATE, gm/sec ARGON
○	6.34	1100	3.65
□	3.34	290	3.65
△	3.16	550	1.45
⌂	4.89	780	3.65
▽	4.95	1100	19.00